Chinese Journal of Mechanical Engineering

ORIGINAL ARTICLE

Open Access

Lift-Off Effect of Koch and Circular Differential Pickup Eddy Current Probes

Guolong Chen[1*], Zheng Cao[1], Shuaishuai Zhang[1], Ji Wei[1], Wei Gao[1] and Wuyin Jin[1]

Abstract

A flexible or planar eddy current probe with a differential structure can suppress the lift-off noise during the inspection of defects. However, the extent of the lift-off effect on differential probes, including different coil structures, varies. In this study, two planar eddy current probes with differential pickup structures and the same size, Koch and circular probes, were used to compare lift-off effects. The eddy current distributions of the probes perturbed by 0° and 90° cracks were obtained by finite element analysis. The analysis results show that the 90° crack can impede the eddy current induced by the Koch probe even further at relatively low lift-off distance. The peak-to-peak values of the signal output from the two probes were compared at different lift-off distances using finite element analysis and experimental methods. In addition, the effects of different frequencies on the lift-off were studied experimentally. The results show that the signal peak-to-peak value of the Koch probe for the inspection of cracks in 90° orientation is larger than that of the circular probe when the lift-off distance is smaller than 1.2 mm. In addition, the influence of the lift-off distance on the peak-to-peak signal value of the two probes was studied via normalization. This indicates that the influence becomes more evident with an increase in excitation frequency. This research discloses the lift-off effect of differential planar eddy current probes with different coil shapes and proves the detection merit of the Koch probe for 90° cracks at low lift-off distances.

Keywords Eddy current testing, Differential pickup probe, Fractal Koch curve, Flexible eddy current probe

1 Introduction

Eddy current (EC) testing (ECT), which is one of the common non-destructive testing (NDT) methods, is widely used to detect defects on the surface or subsurface of metal materials [1, 2]. This method not only plays a key role in the inspection of defects but can also obtain information about their structure and state. When ECT systems are utilized for detection, the EC probe, which can acquire electrical signals fed back from the tested specimen, is their indispensable part. Among the EC probes proposed by scholars worldwide, recently, a probe fabricated using a flexible printed circuit board has exhibited merits such as bendability and ductility. It can fit components with complex geometries to suppress lift-off noise [3, 4].

Aiming at different testing objectives, flexible EC probes and coil structures can be designed so that they can be wound into the most appropriate shape to meet inspection demands. For instance, flexible EC probes with a rectangular coil structure were proposed for the inspection of metal pipes [5], steel balls [6], welded components, and hollow axle inner surfaces [7, 8]; a rosette-shape probe for monitoring the fatigue crack of bolt holes [9]; a butterfly-shape probe for the inspection of screw threads [10]; a probe arranged as parallel and staggered for the inspection of the blades of steam turbines [11]; and a zigzag-shape array probe for the inspection of engine blades [12].

In addition to the above-mentioned probes for practical applications, many flexible or planar EC probes have

*Correspondence:
Guolong Chen
cgl20061273@126.com
[1] School of Mechanical and Electrical Engineering, Lanzhou University of Technology, Lanzhou 730050, China

been manufactured for fundamental research. She et al. [13] proposed a flexible floral EC probe with a spiral coil structure for detecting flaws in a metal plate and adopted a differential coil structure to suppress the lift-off noise and background signal. Zhang et al. [14] presented a three-phase excitation planar EC array probe whose array element was wound with a spiral coil. This probe could detect cracks with a length of 2.5 mm. A planar probe with a differential-structure excitation coil was designed by Chen et al. [15], which had a relatively high detectability of cracks, even at a high lift-off distance.

However, the planar EC probes mentioned above may neglect short cracks whose orientations are almost parallel to the EC. This problem has two possible solutions. One is a planar probe that can induce a rotating EC in a specimen, as proposed by Rosado et al. [16]. This probe consists of an excitation coil with a cross-shaped structure and four pick-up elements arrayed in the quadrants of the cross-shaped structure. When the two excitation traces are fed into currents with same amplitude and 90° phase difference, the EC can be modified dynamically to form a rotating field effect. As a result, the probe can adapt better to changes in the crack orientation. Another solution is to use a planar EC probe based on the Koch fractal curve, as proposed by Chen et al. [17–20]. As the EC induced by the probe is distributed in more orientations, it can enhance the perturbation of the crack in specific orientations toward the EC.

In addition, it should be noted that there is always a lift-off distance between the probe and specimen during practical detection, which may affect the perturbation. Thus, the impact of the lift-off distance on the detection result, namely, the lift-off effect, cannot be ignored. The lift-off effect has been studied for several years. Some studies have been conducted to weaken the adverse influence of the lift-off effect on detection results. To reduce the lift-off effect in pulsed ECT, Tian et al. [21] proposed a method that used normalization and two reference signals. The differential signals were calculated in two stages: The first stage was used to reduce the lift-off effect, and the second stage was used to extract the defect characteristics. Yang et al. [22] transformed the transient response signal of a pulsed EC into the frequency domain to reduce the lift-off effect. Ona et al. [23] optimized the distance between the driver and pick-up coils to suppress lift-off noise, thereby improving crack detection sensitivity. To reduce the lift-off effect fluctuations and improve detection accuracy, Huang et al. [24] proposed a partial least square algorithm combined with support vector machine. However, some studies have explored the lift-off characteristics of probes and improved their detectability. Huang et al. [25] analyzed the lift-off effect of an EMAT system through simulations and experiments to optimize the lift-off distance of the transmitter. Li et al. [26] studied the lift-off effect of a U-shaped ACFM system to obtain a suitable lift-off distance considering both sensitivity and stability. Yin et al. [27] explored the lift-off effects of coplanar capacitive imaging sensors. Zhang et al. [28] analyzed the lift-off effect on a TR probe and presented features for lift-off estimation. Tian et al. [29] utilized the lift-off variance characteristic to estimate the conductivity of samples. Wen et al. [30] made use of the feature of lift-off point of intersection to measure the coating thickness and achieved a comparatively accurate thickness, with 4.9% relative error.

The lift-off effect has not yet been studied as an important factor influencing the detectability of the Koch probe. The previously proposed absolute Koch probe is sensitive to lift-off invariance [17, 19]. In addition, differential-mode interference occurs in the differential-excitation Koch probe [18, 20]. Thus, this article proposes an improved probe called the Koch differential pickup EC probe and aims to study the influence of lift-off distance on the signal output from the probe, and this influence is considered as the lift-off effect. A circular coil probe of the same size and winding method is also presented for comparison with the lift-off effect of the Koch probe. The lift-off effects at different frequencies were investigated.

In this study, first, the coil structures of Koch and circular probes and their principles were determined. Finite-element models were established to analyze the lift-off effect at an excitation frequency of 100 kHz. Subsequently, the finite element results were validated experimentally. Finally, the lift-off effects at different frequencies were experimentally determined.

2 Methodology

2.1 Probe and Specimen

Figure 1(a) shows the coil structure of the Koch differential pickup EC probe. The excitation coil of the probe is a one-turn Koch curve of second order, and the side of the coil is cut to elicit two nodes for connection with the excitation circuit. The pickup coil consists of Koch curves of the same size, which are symmetrical and inversely connected. Then, the two nodes of the pickup

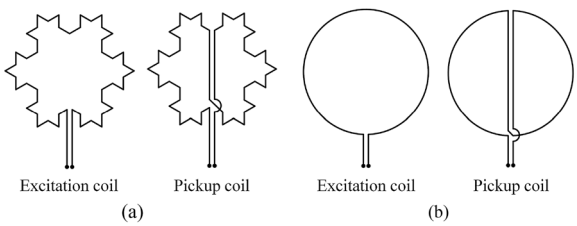

Figure 1 Coil structure of (**a**) Koch probe and (**b**) circular probe

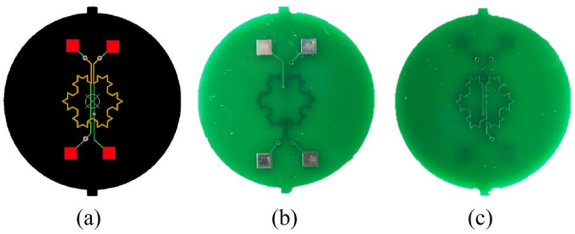

Figure 2 (**a**) Layout, (**b**) front side, and (**c**) rear side of the Koch probe

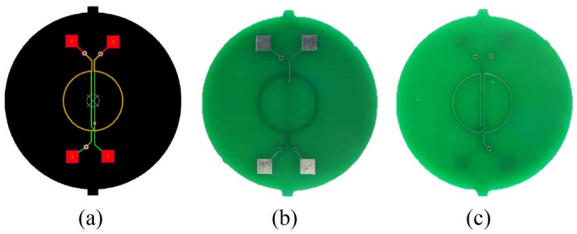

Figure 3 (**a**) Layout, (**b**) front side, and (**c**) rear side of the circular probe

coil are connected to the signal conditioning system. The coil-winding method of the circular differential pickup EC probe, shown in Figure 1(b), is the same as that of the Koch probe. Hereafter, the Koch and circular differential pickup EC probes are called the Koch probe and circular probe, respectively.

As shown in Figures 2 and 3, the two probes are fabricated using a rigid printed circuit board (PCB). Figure 2(a) shows the coil layout of the Koch probe drawn using Altium designer software. The front and rear sides of the PCB-based probe are shown in Figures 2(b) and (c), respectively. The excitation and pickup coils were laid out on the second and fourth PCB, respectively, and the

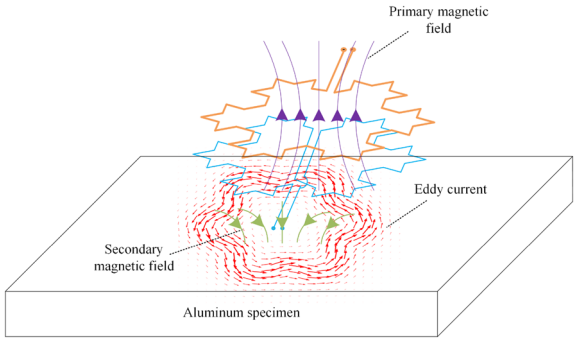

Figure 4 Principle of the Koch differential pickup probe

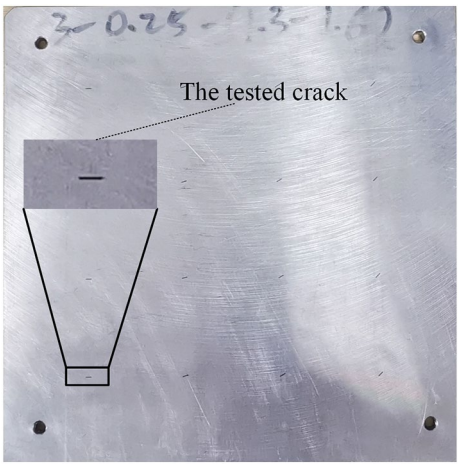

Figure 5 Photograph of the specimen

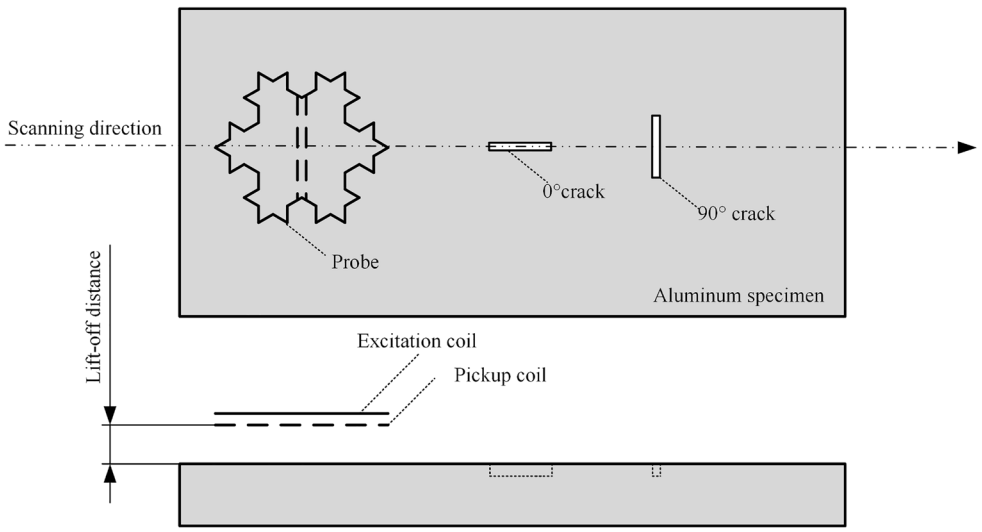

Figure 6 Scanning process for a crack in two orientations

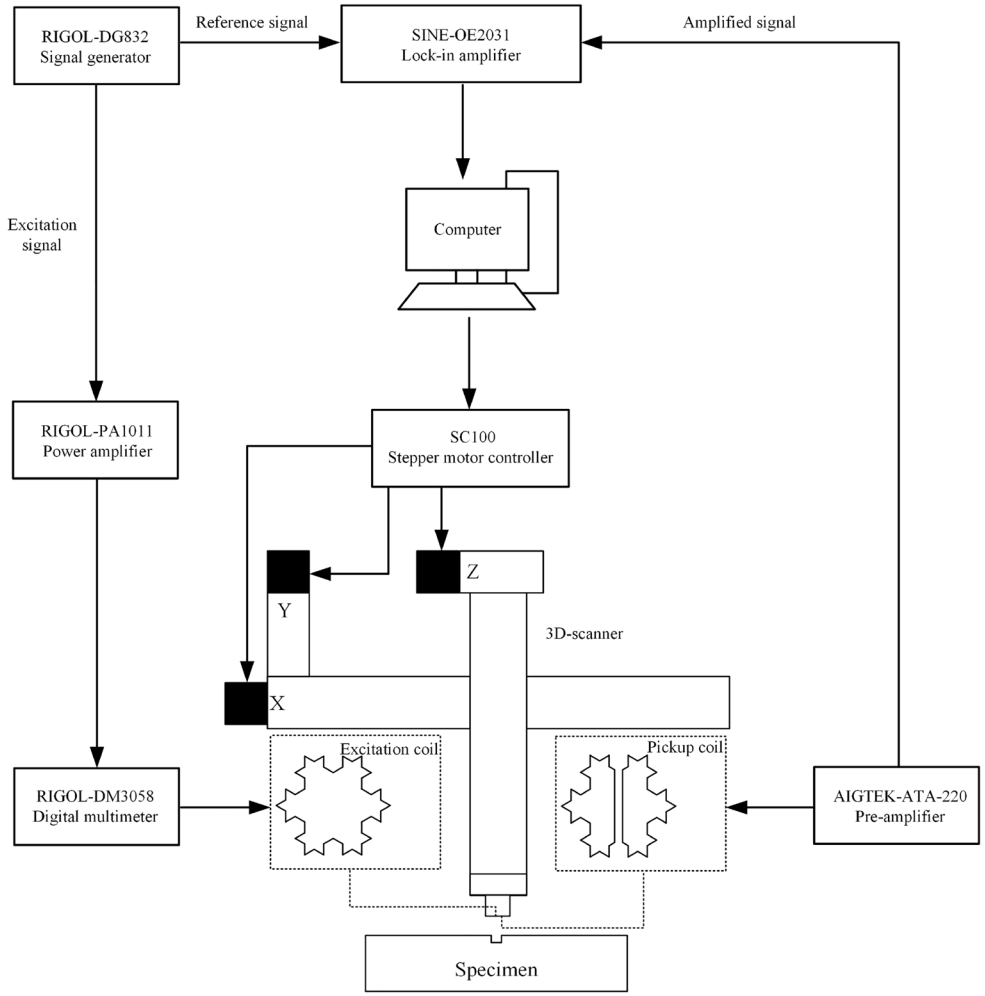

Figure 7 Principle of the experimental system

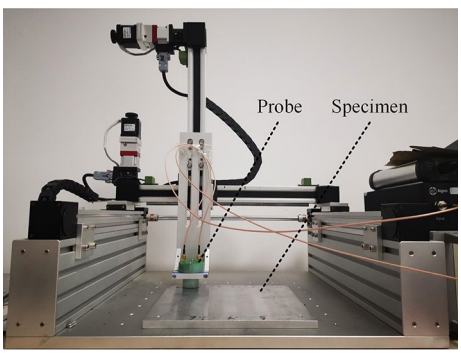

Figure 8 3D-scanner

gap between the two coils was 0.4 mm. The wire widths of the excitation and pickup coils were 0.25 and 0.15 mm, respectively. The nodes of each coil reached the bonding pad through a via hole. The circumcircular diameter of the Koch coil is 10 mm. Figure 3 shows the layout and a photograph of the circular probe, whose layout method and fabrication parameters are the same as those of the Koch probe, and the diameter of its coil is 10 mm.

The working process of the Koch probe is illustrated in Figure 4, which displays the principle of the differential pickup probe. When fed with an alternating current, the excitation coil of the Koch probe generates a primary magnetic field. When the probe approaches the aluminum specimen, the specimen generates a primary magnetic field and induces an EC. Because the EC is also an alternating current, according to Lenz's law, a secondary magnetic field that hampers the change in the primary magnetic field emerges around it. The resultant magnetic field is then generated by the interaction between the primary and secondary magnetic fields. Subsequently, the resultant magnetic field is obtained by the pickup coil, producing an electromotive force. Owing to the special winding method of the pickup coil, the signals

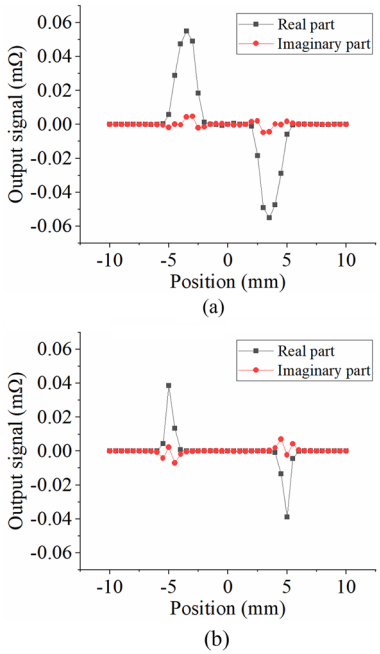

Figure 9 Output signals when the two probes detect a 90° crack at 0.1 mm lift-off distance: (**a**) Koch probe, (**b**) Circular probe

output from the left and right halves are inverse and cancel each other out. When there are no defects under the probe, the signal output from the pickup coil reaches zero, that is, the self-nullifying property under ideal conditions. However, when the probe passes a defect, the signal output from half of the pickup coil is disturbed. At this time, the total output signal of the pickup coil is no longer zero; thus, the defect information can be identified. Owing to this property, the negative influence of the lift-off effect on the probe can be reduced.

In general, the equivalent transimpedance (ET) value of a probe is regarded as its output signal and detectability characterization of the probe. The change in its value reflects the effect of the EC probe on the output signal. This value can be expressed as follows:

$$\dot{Z} = \frac{V_{\mathrm{P}}}{I_{\mathrm{e}}} = \mathrm{Re}\left(\frac{V_{\mathrm{P}}}{I_{\mathrm{e}}}\right) + j\mathrm{Im}\left(\frac{V_{\mathrm{P}}}{I_{\mathrm{e}}}\right), \tag{1}$$

where V_{P} is the induced electromotive force of the pickup coil, j is the imaginary unit, and I_{e} is the excitation current. $\dot{Z}$ is a phasor comprising real and imaginary parts.

The aluminum specimen used in the experiment is shown in Figure 5. Its dimension is 240 mm × 240 mm × 10 mm. Four threaded holes were distributed at the four corners of the specimen and fixed on a 3D scanner. In this study, an artificial crack with dimensions of 3 mm × 0.25 mm × 1.6 mm was selected as the test object.

Figure 6 shows a schematic in which the Koch probe scans the cracks. The crack parallel to the scanning orientation of the probe is the 0° crack, whereas the crack perpendicular to the scanning orientation is the 90° crack. To study the lift-off effect of the proposed probes, the lift-off distance in the experiment ranges from 0.1 mm to 2.0 mm, with 0.1 mm intervals.

2.2 Experimental System

Figure 7 illustrates the principles of the experimental system. First, a signal generator (RIGOL-DG832) emits a sinusoidal signal at 100 kHz. The signal is amplified using a power amplifier (RIGOL-PA1011). Subsequently, a digital multimeter (RIGOL-DM3058) is used to monitor the excitation current. The SMA connector elicited from the probe is linked to the entire circuit in series. This is the excitation part of the process. The signal pickup part follows another path. The signal output from the pickup coil is amplified 1000 times using a preamplifier (AIGTEK-ATA-220) and then entered into the input of a lock-in amplifier (SINE-OE2031). The entered signal is calculated using the reference signal output from the signal generator in the lock-in amplifier to obtain the final output signal. Finally, a computer software is used to communicate with the lock-in amplifier, thereby acquiring the final output signal. In the experiment, the probe was fixed to the Z-axis of the lifting platform of a 3D scanner. The specimen was then placed under the probe as shown in Figure 8. To implement the scanning process of the probe on the crack, the displacement of the 3D scanner in the X-, Y-, and Z-orientations was controlled via communication between the ICM and a stepper motor controller (SC100). The key parameter, the lift-off distance, was adjusted along the Z-axis. When the Z-axis was moved by two impulses equivalent to a negative orientation, the lift-off distance increased by 0.1 mm.

3 Results and Discussions

3.1 Finite Element Analysis

To study the lift-off effect of the Koch and circular probes, finite element models of the two probes were built using COMSOL Multiphysics software at different lift-off distances. The modeling method and parameter settings were the same as those described in Ref. [18].

Figure 9 shows the signal output from the two probes when a 90° crack was detected at a lift-off distance of 0.1 mm. The amplitude of the signal was calculated from the results of the finite element analysis. As can be observed from the figure, the signal amplitude of the real part is larger than that of the imaginary part and has more obvious peaks and troughs, which characterize the

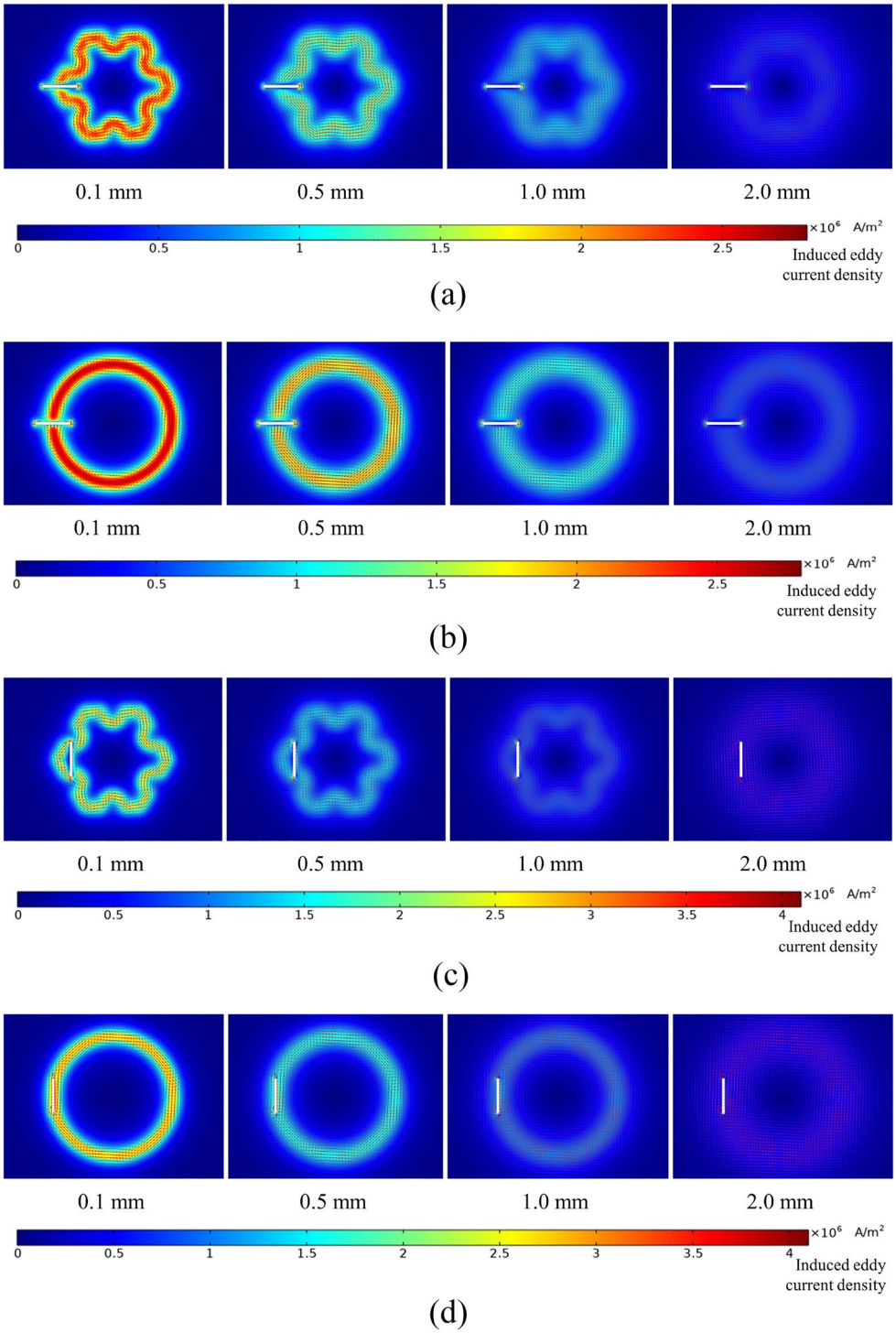

Figure 10 EC distributions disturbed by 0° and 90° cracks at different lift-off distances: (**a**) Koch-0°, (**b**) Circle-0°, (**c**) Koch-90°, (**d**) Circle-90°

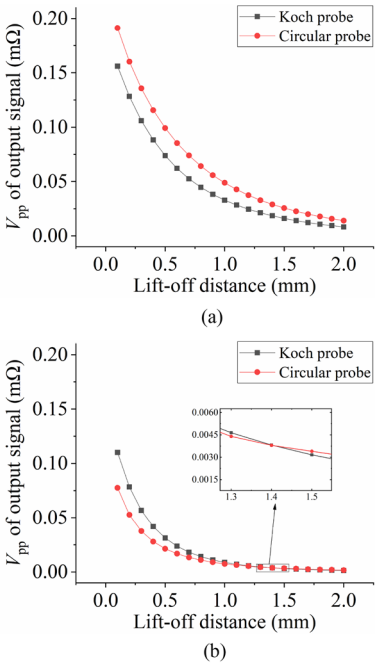

Figure 11 Results of finite element analysis: (**a**) Detection of 0° crack, (**b**) Detection of 90° crack

crack signal. The peak-to-peak value (V_{pp}) of the real part signal represents the response of the probes to the crack. Therefore, the V_{pp} value of the real part of the signal was considered as the detectability of the probes.

Using the post-processing of COMSOL Multiphysics software, EC distributions located in the *xoy* plane and 0.01 mm under the surface of the specimen were obtained. Figure 10 shows the perturbation of the EC due to cracks. Here, 0.1, 0.5, 1.0, and 2.0 mm lift-off distances are taken as examples to observe their EC distributions. When the lift-off distance is relatively small, the EC distribution is similar to that of the excitation coil. However, the EC distribution becomes progressively looser and the EC density decreases with an increase in lift-off distance. When the lift-off distance reaches 2.0 mm, it is difficult to observe the EC distribution. By this time, the interaction between the crack and the EC is extremely weak, which results in a weak signal for the inspection of the crack. In addition, the EC distribution is more evident when a 0° crack is detected at a certain lift-off distance. However, the maximum EC density for the inspection of a 90° crack is higher than that for the inspection of 0° crack.

The V_{pp} value of the real part of the signal was extracted at every lift-off distance, as shown in Figure 11. Figure 11(a) is the result of the detection of a 0° crack with the two probes. As the lift-off distance increases, V_{pp} of the output signal exponentially declines. The V_{pp} value of the signal output from the circular probe for the

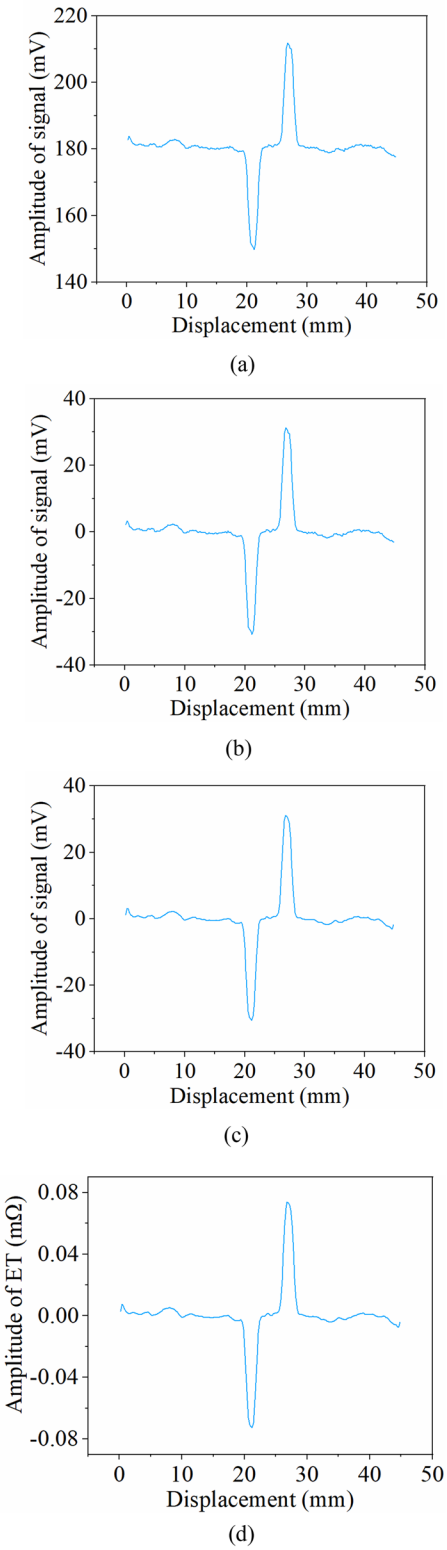

Figure 12 Processing of experimental signal: (**a**) Original signal, (**b**) Signal after detrending, (**c**) Signal after smoothing, (**d**) Equivalent impedance value of the signal

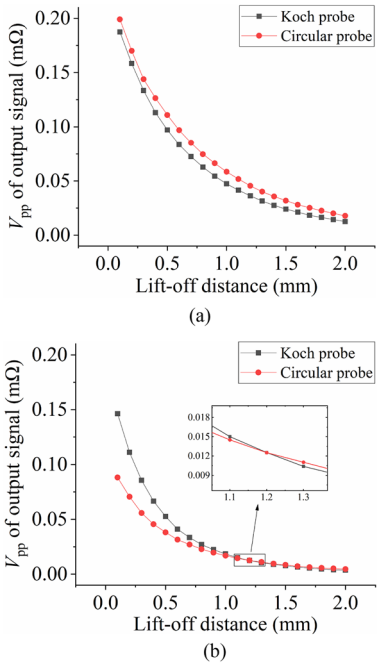

Figure 13 Experimental results: (**a**) Detection of 0° crack, (**b**) Detection of 90° crack

inspection of the 0° crack is higher than that from the Koch probe. When the lift-off distance is approximately 0.8 mm, the crack can be detected steadily, and the signal is relatively obvious.

Figure 11(b) shows the detection results of a 90° crack with the two probes at different lift-off distances. In the figure, the V_{pp} value of the signal output from the two probes decreases exponentially with an increase in lift-off distance. Additionally, the influence of the lift-off distance on the signal of the Koch probe is more evident than that of the circular probe. When the pickup coil of the Koch probe leaves the surface of the specimen, V_{pp} changes at a relatively high speed. Over time, the V_{pp} value of the signal output from the Koch probe is larger than that of the circular probe, thereby showing an apparent detection advantage. As the lift-off distance reaches approximately 1.4 mm, the two lines of V_{pp} intersect. The V_{pp} value of the signal of the circular probe becomes larger than that of the Koch probe when the lift-off distance is more than 1.4 mm. However, the inspection of the two probes for the crack enters the zone with a low signal-to-noise ratio (SNR) because the V_{pp} values of the two probes approach zero and are adjacent. It is difficult to determine whether the circular probe has an evident advantage compared to the Koch probe.

3.2 Experimental Results

To validate the effectiveness of the simulation results, the signals from the experiments were compared. Prior to this, the original experimental signals were processed. Figure 12 shows the steps of the signal process. Figures 12(a), (b), and (c) show the original signal, the signal after detrending, and the signal after filtering, respectively. Then, the signal after filtering was divided by the magnitude of the excitation current and amplification times to obtain the ET, as shown in Figure 12(d). The V_{pp} of the ET was considered the signal characterization of the two probes.

The experimental results of the inspection of the cracks in 0° and 90° orientations is depicted in Figure 13. Figure 13(a) shows the V_{pp} of the output signal for the inspection of the crack in 0° orientation. In general, the value decreases exponentially as the lift-off distance increases, and the response signals output from the two probes are almost at the same level at the same lift-off distance.

In terms of the crack in 90° orientation, the experiment result is consistent with the finite element analysis as displayed in Figure 13(b). The V_{pp} values of the output signal of the two probes decrease exponentially, and the V_{pp} of the circular probe reduces more slowly with the increase in lift-off distance. Similar to the finite element result, the influence of lift-off distance on the signal V_{pp} of the Koch probe is more obvious than that of the circular probe. That is, the detection result of the circular probe is stabler with a small lift-off distance. The V_{pp} values of the signal output from the Koch probe are apparently larger than those of circular probe in a certain lift-off distance range. When the lift-off distance is 0.1 mm, the V_{pp} of the Koch probe is 66.0% larger than that of the circular probe. With the increase in the lift-off distance, the V_{pp} of the Koch probe is no longer larger than that of the circular probe until the lift-off distance is over 1.2 mm.

In the above output signals, the SNR always exists, although the signal is processed using the method shown in Figure 12. Here, the ET signals at a high lift-off distance are presented, indicating that the crack signal is still relatively obvious. The SNR of ET signals were also calculated. The V_{pp} of every signal calculated from the first 14 mm probe displacement and last 14 mm one was set as S_1, and the V_{pp} of the crack signal was set as S_2. The SNR can be formulated using Eq. (2):

$$\mathrm{SNR} = \frac{S_2}{S_1}. \tag{2}$$

Figure 14 shows the SNR of the signal output from the Koch probe. When the 0° crack is detected at 0.1 and 2.0 mm, the SNRs are 17.685 and 5.953, respectively. When the 90° crack is detected at 0.1 and 2.0 mm, the

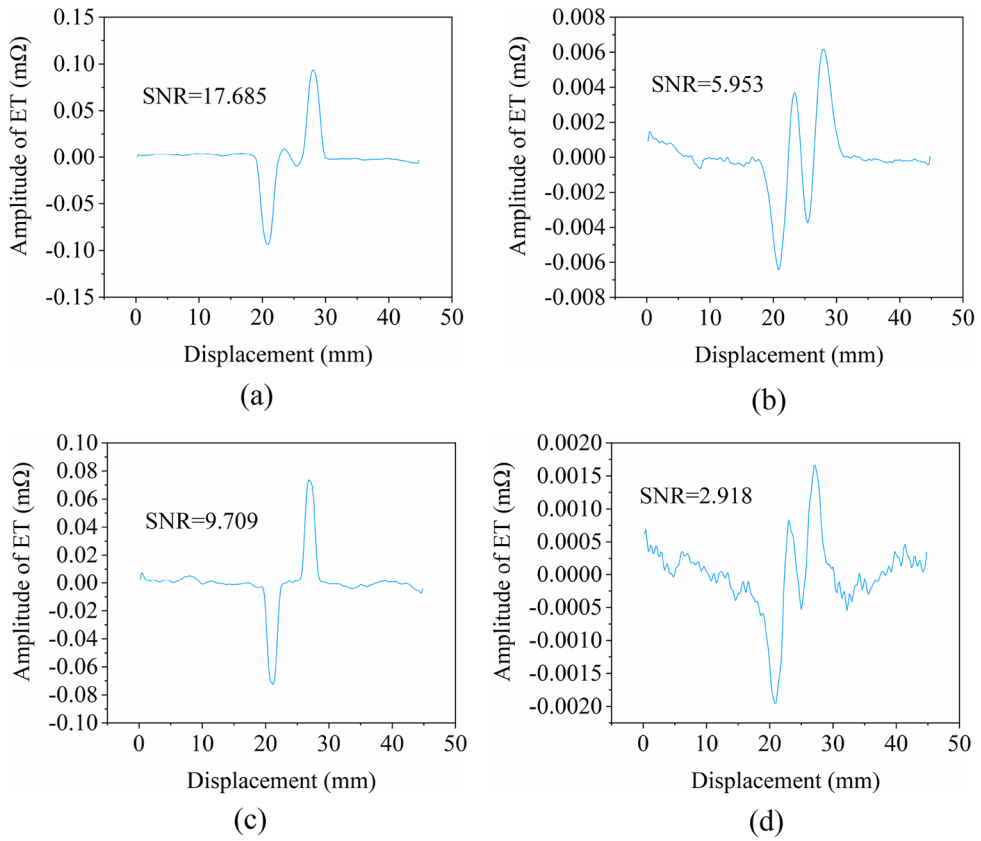

Figure 14 Signal-to-noise ratio (SNR) of Koch probe at 100 kHz: (**a**) 0.1 mm lift-off distance when detecting 0° crack, (**b**) 2.0 mm lift-off distance when detecting 0° crack, (**c**) 0.1 mm lift-off distance when detecting 90° crack, (**d**) 2.0 mm lift-off distance when detecting 90° crack

SNRs are 9.709 and 2.918, respectively. This indicates that a higher SNR can be obtained at low lift-off distance and the SNR of the 0° crack signal is better than that of the 90° crack signal.

3.3 Lift-off Effect at Different Frequencies

It can be concluded from the above results that the V_{pp} value of the signal output from the Koch probe is larger than that of the circular probe when a crack at 90° is detected at 100 kHz excitation frequency. To verify that the Koch probe possesses the same features at different frequencies, an experiment for detecting a 90° crack was carried out at 500 and 1000 kHz.

The V_{pp} values of the signals output from the two probes were obtained at frequencies of 500 and 1000 kHz, as shown in Figure 15. Compared to the detection signals at 100 kHz, the V_{pp} values of the signals output from the two probes increase with a small lift-off distance. While the lift-off distance is 0.1 mm, the V_{pp}, of the Koch probe is 100.7% larger than that of the circular probe at 500 kHz frequency, and the V_{pp} of the Koch probe is 134.5% larger than that of the circular probe at 1000 kHz frequency. However, when the lift-off distance of the Koch probe is larger than 0.1 mm and smaller than 0.5 mm, the V_{pp} values are more susceptible to the lift-off distance, which is a disadvantage for the quantitative identification of cracks. Therefore, it is better to set the lift-off distance at a suitable value, slightly larger than 0.5 mm at excitation frequencies of 500 and 1000 kHz, to ensure both a relatively large V_{pp} (with high SNR) and stability.

Nevertheless, the intersection points between the V_{pp} curves of the two probes in each image are different. For a frequency of 500 kHz, the V_{pp} of the signal output from the circular probe is larger than that from the Koch probe for the first time at 1.8 mm lift-off distance. However, the changes in the two curves fluctuate in the next stage; thus, they tend to be close to each other. For the 1000 kHz frequency, the first time when the V_{pp} of the signal output from the circular probe is larger than that of the Koch probe appears at a 1.5 mm lift-off distance. Then, a fluctuation emerges when the lift-off distance is over 1.5 mm, resulting in a fuzzy relative relationship between the V_{pp} values of the two probes.

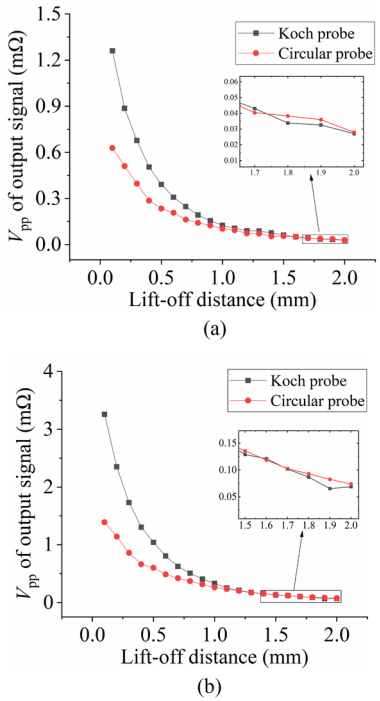

Figure 15 Experimental results at different excitation frequencies: (**a**) 500 kHz, (**b**) 1000 kHz

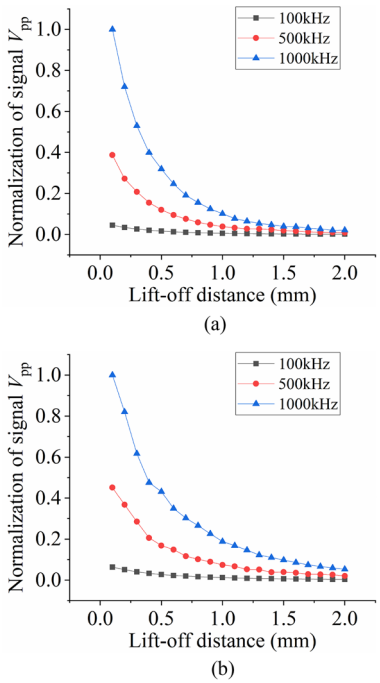

Figure 16 Normalization results at different frequencies: (**a**) Koch probe, (**b**) Circular probe

Moreover, it is worth noticing that the influence of the lift-off distance on the V_{pp} of the Koch probe is more evident than that of the circular probe at frequencies of 100, 500, and 1000 kHz when the 90° crack is scanned. However, it is difficult to observe the lift-off effect of a single probe at different frequencies. Hence, the V_{pp} of the output signals was normalized to study the influence of different frequencies on the lift-off effect of each probe.

Figures 16(a) and (b) show the normalization results of the signal output from the Koch and circular probes, respectively, when the 90° crack was detected. The lift-off effect becomes increasingly evident with an increase in the excitation frequency, and the descent rate of the normalization value of 1000 kHz is faster than that of the other frequencies with an increase in the lift-off distance.

Pulsed-ECT possesses rich frequency components that can provide additional defect information. However, because the coil has only one turn, it is difficult to use a pulsed signal as an excitation source in Koch and circular probes to achieve high sensitivity.

4 Conclusions

This study proposes a planar differential pickup EC probe based on the Koch fractal curve. The probe was wound via a differential structure, which efficiently suppressed lift-off noise during the detection process. A circular differential pick-up EC probe of the same size was designed to compare the lift-off effects of the two probes. From the finite element analysis and experiments, it can be concluded that:

(1) The perturbation of the 90° crack on the Koch probe is stronger than that on the circular probe at low lift-off distance.

(2) The Koch probe is much better than the circular probe for the inspection of V_{pp} cracks in 90° orientation when the lift-off distance is smaller than 1.2 mm.

(3) The influence of the lift-off distance on the signal V_{pp} of 1000 kHz is more evident than that of 100 and 500 kHz.

In the future, our work will focus on the influence of Koch probe coil parameters, such as the coil gap and turns, on the lift-off effect.

Acknowledgements
Not applicable.

Authors' Contributions
GC and ZC carried out the study; ZC wrote the manuscript; SZ and JW assisted with sampling and laboratory analyses; GC, WG and WJ reviewed the manuscript. All authors read and approved the final manuscript.

Funding
Supported by Gansu Provincial Natural Science Foundation of China (Grant No. 22JR5RA229), National Natural Science Foundation of China (Grant Nos. 51807086, 12162021), Hongliu Youth Found of Lanzhou University of Technology and Gansu Provincial Outstanding Graduate Student Innovation Star of China (Grant No. 2021CXZX-453).

Data availability

The data that support the findings of this study are available on request from the corresponding author, upon reasonable request.

Declarations

Competing Interests

The authors declare no competing financial interests.

Received: 11 January 2022 Revised: 27 March 2024 Accepted: 3 April 2024
Published online: 06 May 2024

References

[1] J Garcia-Martin, J Gomez-Gil, E Vazquez-Sanchez. Non-destructive techniques based on eddy current testing. *Sensors (Basel)*, 2011, 11: 2525-2565.
[2] Y WANG, Y Q Niu, Y T Wei, et al. Multi-frequency imaging with non-linear calibration of magnetoresistance sensors for surface and buried defects inspection. *NDT & E International*, 2022, 132: 1-8.
[3] N Zhang, C F Ye, L Peng, et al. Eddy current probe with three-phase excitation and integrated array tunnel magnetoresistance sensors. *IEEE Transactions on Industrial Electronics*, 2021, 68: 5325-5336.
[4] N Zhang, L Peng, X C Tao, et al. Flexible ECT probe with front-end differential setting for inspection of curved CFRP structures. *Composistes Part B*, 2021, 227: 1-13.
[5] Q P Ma, B Gao, G Y Tian, et al. High sensitivity flexible double square winding eddy current array for surface micro-defects inspection. *Sensors and Actuators A: Physical*, 2020, 309: 1-13.
[6] H Y Zhang, L Y Ma, F Q Xie. A method of steel ball surface quality inspection based on flexible arrayed eddy current sensor. *Measurement*, 2019, 144: 192-202.
[7] T Chen, Y T He, J Q Du. A high-sensitivity flexible eddy current array sensor for crack monitoring of welded structures under varying environment. *Sensors (Basel)*, 2018, 18(1780): 1-16.
[8] Z G Sun, D Cai, C Zou, et al. A flexible arrayed eddy current sensor for inspection of hollow axle inner surfaces. *Sensors (Basel)*, 2016, 16(952): 1-9.
[9] G L Chen, W M Zhang, Z J Zhang, et al. A new rosette-like eddy current array sensor with high sensitivity for fatigue defect around bolt hole in SHM. *NDT & E International*, 2018, 94: 70-78.
[10] S B She, Y Z Liu, S J Zhang, et al. Flexible Differential butterfly-shape eddy current array sensor for defect detection of screw thread. *IEEE Sensors Journal*, 2021, 21(18): 20764-20777.
[11] W P Zhang, C L Wang, F Q Xie, et al. Defect imaging curved surface based on flexible eddy current array sensor. *Measurement*, 2020, 151: 1-10.
[12] R F Xie, D X Chen, M C Pan, et al. Fatigue crack length sizing using a novel flexible eddy current sensor array. *Sensors (Basel)*, 2015: 32138-32151.
[13] S B She, Y Z He, Y F Chen, et al. Flexible floral eddy current probe for detecting flaws in metal plate. *IEEE Sensors Journal*, 2020, 20(18): 10521-10529.
[14] N Zhang, C F Ye, L Peng, et al. Novel array eddy current sensor with three-phase excitation. *IEEE Sensors Journal*, 2019, 19(18): 7896-7905.
[15] K F Chen, B Gao, G Y Tian, et al. Differential coupling double-layer coil for eddy current testing with high lift-off. *IEEE Sensors Journal*, 2021, 21(16): 18146-18155.
[16] L S Rosado, T G Santos, P M Ramos, et al. A new dual driver planar eddy current probe with dynamically controlled induction pattern. *NDT & E International*, 2015, 70: 29-37.
[17] G L Chen, W M Zhang, W H Pang. Koch curve fractal geometry excitation probe for eddy current non-destructive testing. *Measurement*, 2018, 124: 470-478.
[18] G L Chen, Z Cao, W M Zhang. A novel planar differential Koch fractal eddy current probe with parallel wound topological structure. *Journal of Sensors*, 2021: 1-13.
[19] G L Chen, S S Zhang, Z Cao, et al. Research on crack detection performance of absolute Koch planar eddy current sensor. *Chinese Journal of Scientific Instrument*, 2022, 43(10): 98-107. (in Chinese)
[20] G L Chen, Z B Song, W Y Jin. A novel planar differential excitation eddy current probe based on the fractal Koch curve. *Measurement*, 2022, 193: 1-11.
[21] G Y Tian, A Sophian. Reduction of lift-off effects for pulsed eddy current NDT. *NDT & E International*, 2005, 38: 319-324.
[22] B F Yang, B Li, Y J Wang. Reduction of lift-off effect for pulsed eddy current NDT based on sensor design and frequency spectrum analysis. *Nondestructive Testing and Evaluation*, 2010, 25(1): 77-89.
[23] D I Ona, G Y Tian, R Sutthaweekul, et al. Design and optimisation of mutual inductance based pulsed eddy current probe. *Measurement*, 2019, 144: 402-409.
[24] P J Huang, X W Luo, D B Hou, et al. Lift-off nulling and internal state inspection of multi-layer conductive structures by combined signal features in pulsed eddy current testing. *Nondestructive Testing and Evaluation*, 2018, 33(3): 272-289.
[25] S L Huang, W Zhao, Y S Zhang, et al. Study on the lift-off effect of EMAT. *Sensors and Actuators A: Physical*, 2009, 153: 218-221.
[26] W Li, G M Chen, X K Yin, et al. Analysis of the lift-off effect of a U-shaped ACFM system. *NDT & E International*, 2013, 53: 31-35.
[27] X K Yin, C Li, Z Li, et al. Lift-off effect for capacitive imaging sensors. *Sensors (Basel)*, 2018, 18(4286): 1-22.
[28] Q Zhang, X Li, G Y Tian. Analysis of lift-off effect on transmitter-receiver probe in eddy current testing. *Electromagnetic Non-Destructive Evaluation*, 2020, 45: 27-35.
[29] G Y Tian, Y Li, C Mandache. Study of lift-off invariance for pulsed eddy-current signals. *IEEE Transactions on Magnetics*, 2009, 45(1): 184-191.
[30] Y Wang, M B Fan, B H Cao, et al. Measurement of coating thickness using lift-off point of intersection features from pulsed eddy current signals. *NDT & E International*, 2020, 116: 1-12.

Guolong Chen born in 1987, is currently an associate professor at *School of Mechanical and Electrical Engineering, Lanzhou University of Technology, China*. He received his bachelor degree and PhD degree both from *Beijing Institute of Technology, China*, in 2010 and 2018, respectively. His research interests include electromagnetic non-destructive testing and intelligent sensors.

Zheng Cao born in 1998, is currently a PhD candidate at *School of Aerospace Engineering, Xiamen University, China*. He received his bachelor and master degrees both from *Lanzhou University of Technology, China*, in 2019 and 2022, respectively. His research interests include electromagnetic non-destructive testing.

Shuaishuai Zhang born in 1998, is currently a Master candidate at *School of Mechanical and Electrical Engineering, Lanzhou University of Technology, China*. His research interests include electromagnetic non-destructive testing.

Ji Wei born in 1997, is currently a Master candidate at *School of Mechanical and Electrical Engineering, Lanzhou University of Technology, China*. His research interests include electromagnetic non-destructive testing.

Wei Gao born in 1986, is currently a lecturer at *School of Science, Lanzhou University of Technology, China*. He received his PhD degree from *Lanzhou University, China*, in 2018. His current research focuses on characterization of force magnetic coupling properties of magneto-sensitive soft materials.

Wuyin Jin born in 1969, is currently a professor at *School of Mechanical and Electrical Engineering, Lanzhou University of Technology, China*. He received his PhD degree from *Xi'an Jiaotong University, China*, in 2004. His research interests include machine vision and image processing.